Study of the $C(^3P) + OH(X^2\Pi) \rightarrow CO(X^1\Sigma_g^+) + H(^2S)$ Reaction: A Fully Global ab Initio Potential Energy Surface of the X^2A' State

Alexandre Zanchet

Laboratoire PALMS, UMR CNRS 6627, Université de Rennes 1, Campus de Beaulieu, 35042 Rennes Cedex, France

Beatrice Bussery-Honvault* and Pascal Honvault

Laboratoire LPM, UMR CNRS 6624, Université de Franche-Comté, Campus de la Bouloie, 16 route de Gray, 25030 Besançon Cedex, France

Received: July 11, 2006; In Final Form: September 5, 2006

The $C(^3P) + OH(X\ ^2\Pi) \rightarrow CO(X\ ^1\Sigma_g^+) + H(^2S)$ reaction has been investigated by ab initio electronic structure calculations of the X^2A' state based on the multireference (MR) internally contracted single and double configuration interaction (SDCI) method plus Davidson correction (+Q) using Dunning aug-cc-pVQZ basis sets. In particular, the multireference space is taken to be a complete active space (CAS). Improvement over previously proposed potential energy surfaces for HCO/COH is obtained in the sense that present surface describes also the potential part where the CO interatomic distance is large. A large number of geometries (around 2000) have been calculated and analytically fitted using the reproducing kernel Hilbert space (RKHS) method of Ho and Rabitz both for the two-body and three-body terms following the many-body decomposition of the total electronic energies. Results show that the global reaction is highly exothermic (∼6.4 eV) and barrierless (relative to the reactant channel), while five potential barriers are located on this surface. The three minima and five saddle points observed are characterized and found to be in good agreement with previous work. The three minima correspond to the formation of HCO and COH complexes and to the CO + H products, with the COH complex being a metastable minimum relative to the product channel. The five saddle points correspond to potential barriers for both the dissociation/formation of HCO and COH into/from CO + H, to barriers for the isomerization of HCO into COH and to barriers for the inversion of HCO and COH through their respective linear configuration.

I. Introduction

The HCO system has been the object of several experiments spanning a wide energy range, from subthermal of interest in astrophysics, to thermal of interest in combustion studies, to suprathermal of interest in vibrational energy transfer. Furthermore, the OH hydroxyl radical plays a crucial role in the atmospheric chemistry of the troposphere. Indeed, it reacts with a lot of compounds and acts as a cleaner of the atmosphere despite its very short lifetime. It can transform active species into inactive ones or, inversely, transform inactive species into active ones. In addition, because ab initio calculations provide accurate energies for a system of such light atoms, HCO has become a prototype for the theoretical studies of radical spectroscopy or unimolecular reactions. So, there have been previous theoretical studies of the HCO radical in which portions of the potential energy surface have been evaluated by semiempirical or ab initio methods. For instance, the HCO complex has been the object of previous studies concerning its photodissociation process through the $X^2A'-A^2A''$ Renner−Teller coupling.[1−3] The ab initio characteristics of the extrema (3 minima and 5 saddle points) have been improved over the previous values published more than 20 years ago.[4,5] HCO is known to be stable by 0.8 V relative to $H + CO(X^1\Sigma^+)$ with only a small barrier (0.07 eV relative to H + CO) toward dissociation or formation into/from H + CO. On the other hand, COH has never been observed experimentally, but accurate ab initio calculations indicate that a metastable minimum corresponding to COH exists at 1.04 eV above H + CO with a barrier of 0.68 eV to dissociation leading to a barrier of formation of 1.72 eV from H + CO. The sensitivity of the COH formation with the potential barrier was analyzed by quasi-classical trajectory calculations of collisional excitation of CO with H.[6,7] Quantum coupled channel calculations of resonances in H + CO have been conducted by Romanowsky et al.[8] These resonances are observed due to temporary formation of the HCO complex.

Following the methodology previously used for the treatment of reactive collisions between H_2 and open-shell atoms,[9−12] we start to explore here a new class of collisional systems: the studies of reactive collisions between open-shell atoms and the hydroxyl radical, OH. As it involves the presence of two open-shell systems, the experimental studies are particularly scarce, so that present theoretical study is pioneered in the field and will furnish essential information. First of all, we will study the reaction of the hydroxyl radical with a carbon atom in its ground ^3P state leading to the reaction: $C(^3P) + OH(X^2\Pi) \rightarrow CO(X^2\Sigma^+) + H(^2S)$. To our knowledge, it is the first global

* Author for correspondence. E-mail: beatrice.honvault-bussery@univ−fcomte.fr.

10.1021/jp064352p CCC: $33.50
Published on Web 10/06/2006

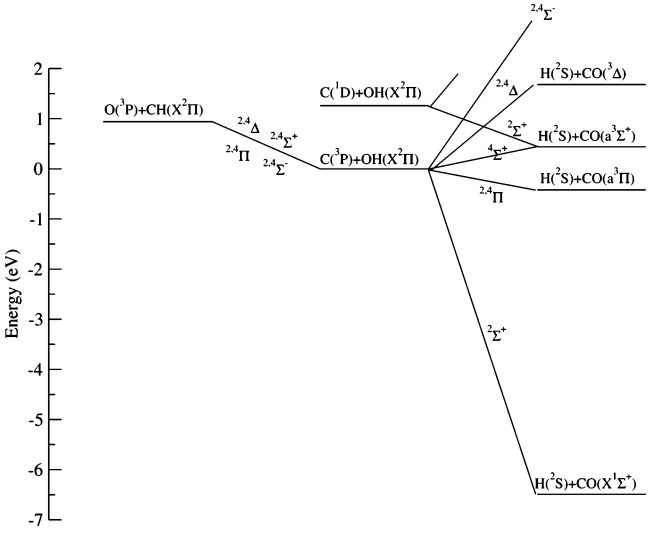

Figure 1. Correlation diagram in $C_{\infty v}$ symmetry.

TABLE 1: Electronic States Arising from the Interaction of A(^{3}P) + BH(X$^2\Pi$) with (A, B) = (C, O) or (O, C), and H(^{2}S) + CO(X$^1\Sigma^+$) Together with Their Correlation Between $C_{\infty v}$ and C_s Point Groups

complex	$C_{\infty v}$	C_s
A(^{3}P) + BH(X$^2\Pi$)	$^{2,4}\Pi$	^{2,4}A′, ^{2,4}A″
	$^{2,4}\Delta$	^{2,4}A′, ^{2,4}A″
	$^{2,4}\Sigma^+$	^{2,4}A′
	$^{2,4}\Sigma^-$	^{2,4}A″
H(^{2}S) + CO(X$^1\Sigma^+$)	$^2\Sigma^+$	^{2}A′

study of this system, as it has never been studied previously either theoretically or experimentally.

II. Ab Initio Electronic Calculations

A. Correlation Diagram. The correlation diagram presented in Figure 1 collects the lowest energetic data available for the entrance and output channels of the title reaction, i.e., for the C, H, and O atoms and the diatoms OH, CO, and CH. The energy differences correspond to values without the zero-point energies. The interaction of C(^{3}P) + OH(X$^2\Pi$) leads to six doublet states and six quartet states which are correlated in $C_{\infty v}$ to $^{2,4}\Sigma^+$, $^{2,4}\Sigma^-$, $^{2,4}\Pi$, and $^{2,4}\Delta$ states as described in Table 1. Each Π and Δ state will split into one A′ and one A″ state in the C_s symmetry group, i.e., when the complex is bent, while the Σ^+ state leads to one A′ and the Σ^- state to one A″ state. So, in C_s, the C + OH interaction will lead to three ^{2}A′ and three ^{2}A″ states. However, not shown on the correlation diagram of Figure 1, most of these states present a repulsive behavior or a very shallow attractive well at large distance between ground-state C and OH, except for the $^2\Pi$ state, which shows an attractive binding between the reactants. The title reaction will be strongly exothermic, as the energetic difference between the reactants and the products, both in their ground states, is 6.49 eV. The excited a$^3\Pi$ state of CO is energetically below the ground-state reactants and is correlated to it via doublet and quartet states. Nevertheless, this state is more than 6 eV above the ground-state products. From Figure 1, we note that only one doublet state correlates to the ground-state products, the X^{2}A′. Crossings of different symmetry states in $C_{\infty v}$ will result in avoided crossing or conical intersection in C_s if the states belong to the same class of symmetry in this group. This will be the case between the $^2\Sigma^+$ and $^2\Pi$ states, as the $^2\Pi$ state is more bound than the $^2\Sigma^+$ in the entrance channel, while only the $^2\Sigma^+$ state correlates to the ground-state products. Indeed, in the study of the dissociation pathway of HCO into CO + H by the group of Werner et al.,[1,2,13] they have informed us that, for collinear geometry, the symmetry of the HCO ground-state wave function is $^2\Pi$ and that it correlates asymptotically with the first excited state of CO, i.e., CO(a$^3\Pi$) + H(^{2}S), while the lowest ground-state products dissociation CO(X $^1\Sigma^+$) + H(^{2}S) correlates with a repulsive (relative to it) $^2\Sigma^+$ state. This leads to a crossing of the $^2\Pi$ and $^2\Sigma^+$ states at a CH distance around 2.6 bohr (see Figure 1 of ref 13), while it will lead to an avoided crossing (saddle point) between the two ^{2}A′ states in C_s. All other excited states of CO ($^3\Sigma^+$, $^{1,3}\Sigma^-$, $^{1,3}\Delta$, and $^1\Pi$) lead to repulsive interaction states with hydrogen (relative to the respective dissociation channel) at linear geometry, except the 2$^2\Pi$ state, which shows a pronounced potential well. We note from the study of Werner and colleagues that the order of the CO excited states changes as a function of the interatomic C−O distance.

B. Computational Details. We have done ab initio calculations of the ground X^{2}A′ state of HCO/COH using the internally contracted MR-SDCI (multireference single and double configuration interaction) method as previously applied for the description of potential energy surfaces (PESs) of the three-atoms complex.[9,14−16] The multireference space is taken as a complete active space (CAS), to correctly describe, i.e., at a size-consistent level, the electronic rearrangements that follows the breaking and forming of chemical bonds occurring during the reaction. The configurations included in the reference wave function are obtained by distributing the valence electrons (2 electrons for carbon, 4 electrons for oxygen, and 1 electron for H) in all possible ways among the valence orbitals, 2p for C and O and 1s for H, resulting in a CAS of 7 electrons distributed in 7 orbitals (5−9a′ and 1−2a″). The 1s and 2s orbitals of C and O (1−4a′) have been treated as inactive at the CAS level and kept doubly occupied. They are not supposed to participate in the bond breaking and forming which occur along the reaction. While the 2s electrons of C and O (3−4a′) have been correlated at the configuration interaction (CI) level, the 1s core (1−2a′) orbitals have been frozen even at the CI level to keep the computer time reasonable. We note that the 9a′ has been included in the present active space, which is different from Werner calculations.[13] The paired and unpaired electrons arrangements of HCO are shown in Figure 2 for the reactants and products and indicate the necessity to include the 9a′ orbital in the active space to have smooth behavior of the potential as the orbital correlates with a CO valence one. The electrons and orbitals of the CAS are entraped in a box in Figure 2, and the triatomic orbitals are numbered and labeled in C_s symmetry. The complete active space self-consistent field (CASSCF) molecular orbitals have been built up by averaging the calculations over the first three states ((1,2)A′ and 1A″) in order to improve the description of the ground state near the dissociation where degeneracy between states occurs. The dynamic correlation has been handled by a calculation at the internally contracted single and double configuration interaction (SDCI) level based on the natural orbitals of the previous CASSCF step. Finally, total energies have been corrected for the non-size consistency by addition of the Davidson correction (noted +Q). All the ab initio calculations presented here have been performed with the *MOLPRO* package.[17] Following previous quality tests with several basis sets made by the group of Werner,[13] we have chosen the polarized correlation consistent basis set of quadruple-ζ quality of Dunning,[18] i.e., contracted basis sets of [5s4p3d2f] for C and O and [4s3p2d] for H. With such basis sets, we have obtained ab initio characteristics (R_e, D_e, ω_e) of the diatomics (OH, CH, and CO) at the MR-SDCI+Q level in

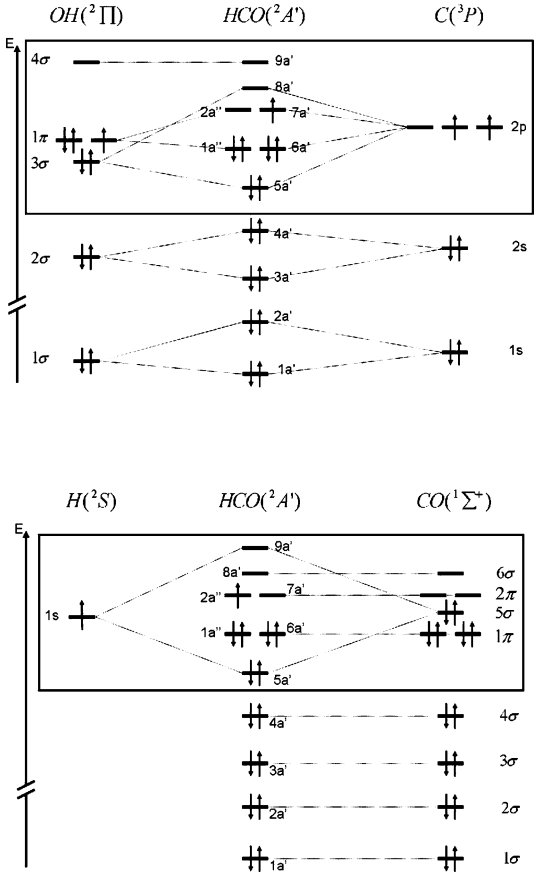

Figure 2. Qualitative energetic diagrams of the HCO molecular orbitals relative to those of the reactants (upper panel) and products (lower panel).

TABLE 2: Ab Initio (MR-SDCI+Q) and Experimental Spectroscopic Constants of CO($X^1\Sigma^+$), CH($X^2\Pi$) and OH($X^2\Pi$)

diatom		R_e (bohr)	D_e (eV)	ω_e (cm^{-1})
CO($X^1\Sigma^+$)	MRCI+Q	2.14	11.03	2162
	fit			
	expt.[a,c]	2.132	11.08	2169.8
CH($X^2\Pi$)	MRCI+Q	2.12	3.58	2860
	fit			
	expt.[b]	2.116	3.65	2858.5
OH($X^2\Pi$)	MRCI+Q	1.83	4.53	3748
	fit			
	expt.[b]	1.834	4.58	3737.8

[a] Ref 19. [b] Ref 20. [c] Ref 21.

TABLE 3: Absolute and Relative to C(^{3}P) + OH($X^2\Pi$) ab initio energies for the Reactant and Product Dissociations[a]

dissociation channel	absolute energy (au)	relative energy (eV)	expt.[b] (eV)
C(^{3}P) + O(^{3}P) + H(^{2}S)	−113.27444262	4.52	4.58
O(^{3}P) + CH($X^2\Pi$)	−113.40631230	0.94	0.93
C(^{3}P) + OH($X^2\Pi$)	−113.44070079	0.0	0.0
H(^{2}S) + CO($a^3\Pi$)	−113.45597973	−0.42	−0.46
H(^{2}S) + CO($X^1\Sigma^+$)	−113.67936223	−6.49	−6.50

[a] The ab initio energies are given at the MR-SDCI+Q level. [b] Ref 20.

good agreement with previous works and in particular with the experimental values presented in Table 2. Similarly, relative electronic energies of the dissociation channels presented in Table 3 are in good agreement with the literature values. The quality of the basis sets is so confirmed by present results.

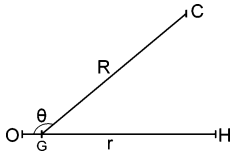

Figure 3. Jacobi coordinates relative to C + OH. The *G* point is fixed at the center of mass of OH.

III. RKHS Fitting Procedure

Following Murrell and Carter,[22] the single-valued potential energy surface for the title reaction can be decomposed in terms of many-body expansion

$$V_{HCO} = V^{(1)} + V^{(2)}_{OH}(R_{OH}) + V^{(2)}_{CO}(R_{CO}) + V^{(2)}_{CH}(R_{CH}) + V^{(3)}_{HCO}(R_{OH}, R_{CO}, R_{CH}) \quad (1)$$

where R_{AB} is the bond distance of the diatom AB, i.e., O−H, C−O, or C−H and $V^{(1)}$, $V^{(2)}$, and $V^{(3)}$ are, respectively, the one-, two-, and three-body terms. The one- and two-body terms are determined separately. The one-body term is assigned the value of the total dissociation energy in the three-atom limit, i.e., $E(C(^3P)) + E(O(^3P)) + E(H(^2S))$. The two-body terms are obtained by interpolating a discrete set of ab initio points. Finally, the three-body term is obtained by interpolating the difference between the total electronic energy and the corresponding one- and two-body terms on an optimized 3D regular grid (N_R, N_r, N_θ) of ab initio points in Jacobi coordinates (R, r, and θ) relative to C + OH (see Figure 3).

A. Two-Body Potentials. For simplicity, we will drop the subscripts OH, CO, and CH in the two-body terms for the moment. It has been shown that within the framework of the reproducing kernel Hilbert space (RKHS) a two-body potential $V^{(2)}(r)$ can be represented as[14]

$$V^{(2)}(r) = \sum_{i=1}^{N} \alpha_i q_1^{n,m}(r_i, r) \quad (2)$$

in terms of a distancelike, *n*th-order, 1D reproducing kernel

$$q_1^{n,m}(r', r) = n^2 B(m+1, n) r_>^{-m-1} {}_2F_1\left(-n+1, m+1; n+m+1; \frac{r_<}{r_>}\right) \quad (3)$$

with integers $n \geq 1$ and $m \geq 0$. $r_>$ and $r_<$ are, respectively, the larger and smaller of r and r', $B(a, b)$ is the β function and ${}_2F_1(a, b; c; z)$ is the Gauss hypergeometric function. The index i of eq 2 runs over the N two-body data points, adopted for the interpolation. It is prudent to keep n and m as low as possible, so that the interpolant of eq 2 can be globally smooth regardless of the number N of data points. Moreover, the interpolation based on eq 2 will be insensitive to the choice of m as long as the spacings between the data points are sufficiently small and the number of points is sufficiently large.[14] As suggested in ref 14, we took $n = 2$ and $m = 0$, so that the interpolation based on eq 2 will be unique. Thus, $q_1^{2,0}$ is

$$q_1^{2,0}(r, r') = \frac{2}{r_>} {}_2F_1\left(-1, 1; 3; \frac{r_<}{r_>}\right) \quad (4)$$

and

$$V^{(2)}(r_i) = \sum_{j=1}^{N} \alpha_j q_1^{2,0}(r_j, r_i) \quad i = 1, ..., N \tag{5}$$

The α_j coefficients for the OH, CO, and CH potentials are available, on request, from the authors.

B. Three-Body Potential. Now, we consider the three-body interaction potential $V_{HCO}^{(3)}(R, r, \theta)$ obtained on a 3D regular grid in Jacobi coordinates (R, r, θ). Again, for simplicity, we will drop the subscript HCO. We have taken the general case where all three numbers N_R, N_r, and N_θ of the optimized 3D regular grid are large, i.e., >10. Here, we introduce three new anglelike variables (x, y, z) with $0 \le x = \exp(-aR) \le 1$, $0 \le y = \exp(-br) \le 1$, and $0 \le z = (1 + \cos\theta)/2 \le 1$, with a and b being two positive real numbers, to account for the fact that the three-body term falls off quickly to zero at large R and r. In the present case, the optimized choice for a and b is 0.4. By invoking the RKHS method,[23,24] the three-body term can be represented as a direct product of three 1D reproducing kernels in x, y, and z. These anglelike reproducing kernels in the intervals [0, 1] can be written in a closed form as

$$q_2^{\,n}(x, x') = \pi_{n-1}(x, x') + \tilde{q}_2^{\,n}(x, x') \tag{6}$$

where $\pi_{n-1}(x, x')$ is the $(n-1)$-order polynomial kernel of the form

$$\pi_{n-1}(x, x') = \sum_{i=0}^{n-1} x^i x'^i \tag{7}$$

and $\tilde{q}_2^{\,n}(x, x')$ is an anglelike reproducing kernel of the form

$$\tilde{q}_2^{\,n}(x, x') = n x_<^n x_>^{n-1} {}_2F_1\left(1, -n+1; n+1; \frac{x_<}{x_>}\right) \tag{8}$$

where $x_>$ and $x_<$ are, respectively, the larger and smaller of x and x'. In terms of the reproducing kernels defined in eqs 6 and 8, the 3D three-body term can be represented as

$$V^{(3)}(x, y, z) = \sum_{i=1}^{N_x}\sum_{j=1}^{N_y}\sum_{k=1}^{N_z} \alpha_{ijk} \tilde{q}_2^{\,n_x}(x_i, x) \tilde{q}_2^{\,n_y}(y_j, y) q_2^{\,n_z}(z_k, z) \tag{9}$$

where $N_x(=N_R)$, $N_y(=N_r)$, and $N_z(=N_\theta)$ denote, respectively, the number of data points in R, r, and θ; and n_x, n_y, and n_z are the orders of the anglelike reproducing kernels. The coefficients α_{ijk} are determined by solving eq 9 on the optimized $N_x \times N_y \times N_z$ regular grid. Here again, the n_x, n_y, and n_z are assumed to be low, i.e., $n_x = n_y = n_z = 2$. In this particular case, the $\tilde{q}_2^{\,n}(x, x')$ kernel reduces to

$$\tilde{q}_2^{\,2}(x, x') = 2x_<^2 x_> \left(1 - \frac{x_<}{3x_>}\right) \tag{10}$$

The potential energy of HCO/COH has been calculated on a three-dimensional grid ($N_R = 16$) × ($N_r = 13$) × ($N_\theta = 10$) of ab initio geometries with R = {1.0, 1.4, 1.6, 1.8, 2.0, 2.2, 2.4, 2.6, 3.0, 3.5, 4.0, 4.5, 5.0, 5.625, 6.25, 7.5}, r = {1.0, 1.4, 1.6, 1.8, 2.0, 2.2, 2.4, 2.6, 3.0, 3.5, 4.0, 4.5, 5.0}, and θ = {0, 30, 50, 60, 90, 120, 135, 150, 155, 180} yielding a total of 2080 nuclear geometries. The α_{ijk} coefficients determined by solving eq 9 are available, on request, from the authors.

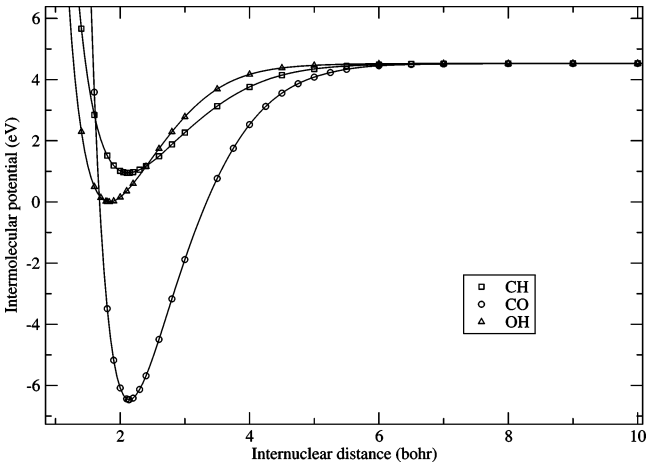

Figure 4. MR-SDCI+Q diatomic potential energy curves (symbols) for OH (triangle up), CO (circle), and CH (square) as a function of the respective internuclear distance together with the related triatomic global fit (solid line) obtained with $R = 50$ bohr for the OH curve, $R_{CO} = 50$ bohr for the CH curve and $R_{CH} = 50$ bohr for the CO one.

It is readily seen that the relative error is zero at each ab initio point, as the RKHS interpolated surface is found to exactly reproduce the points on which it is based. Indeed, we have a root-mean-square error of $\sim 10^{-12}$ eV between the RKHS fit and the ab initio points, which results from the numerical evaluation of the fit. Nevertheless, the constructed PES contains two sources of error due to (i) the finite number of the ab initio data and (ii) the regularization. Ho and Rabitz proposed a way to estimate an a posteriori error bound,[23] but this estimation has not been done in the present work, so that we have no idea of the quality of the present fit outside the ab initio points. Anyway, we can say that the quality of the present PES is limited by the accuracy of the ab initio method (a few kcal/mol) rather than by the fitting procedure which can be as precise as we need.

IV. Results and Discussion

A. Diatomic Potentials. We report in Figure 4 the ab initio MR-SDCI+Q energies of the diatomic potentials associated with the OH, CO, and CH molecules, together with the triatomic global fit when the third atom is far away from the diatom, i.e., $R = 50$ bohr for OH, $R_{CO} = 50$ bohr for CH and $R_{CH} = 50$ bohr for CO. The triple bond in CO leads to a very strong binding of more than twice that in CH or OH. In all three cases, the diatom + atom correlates asymptotically with the atoms in their ground states, i.e., C(^{3}P) + O(^{3}P) + H(^{2}S), so the full PES matches perfectly the diatomic potentials.

The good description of each diatomic potential is further confirmed by the values of Table 2. Indeed, the dissociation energies (D_e) of OH and CO yield a calculated exoergicity ΔE and ΔH_0^0 for the title reaction of 6.5 and 6.4 eV, respectively, in perfect agreement with the respective experimental values derived from Table 2.

B. Global Potential Energy Surface. Figure 5a shows the analytical ground X^2A' PES for a fixed OH distance as a function of the position of the carbon atom around OH describing the potential energy for the reactants. The hydroxyl radical lies on the x-axis with its geometric center fixed at the origin and its interatomic distance fixed at 1.83 bohr. The carbon atom is given by the (x, y) coordinates. The zero of energy is taken to be the entrance channel, C(^{3}P) + OH($X^2\Pi$) ($r_e = 1.83$ bohr). There is no barrier for reaction regardless of the approach angle of the carbon atom to OH, except near 180°, as the

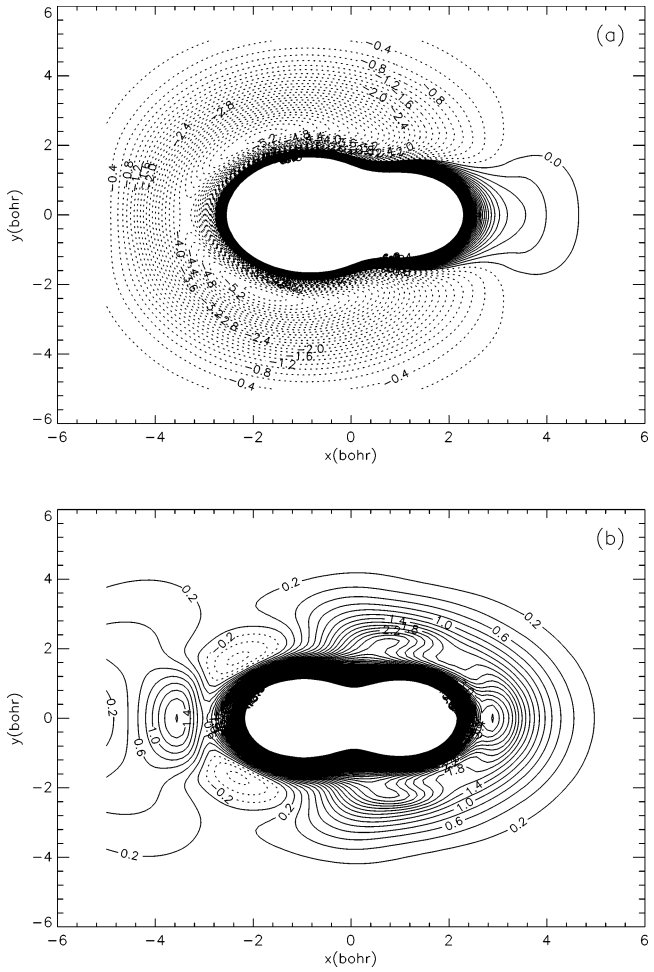

Figure 5. Polar contours of the X^2A' state of COH (a) at a fixed O−H distance, $r_{OH} = 1.83$ bohr, (b) at a fixed C−O distance, $r_{CO} = 2.14$ bohr. The zero energy is taken (a) at the entrance channel, i.e., $C(^3P) + OH(X^2\Pi)$ (r_e), (b) at the exit channel $H(^2S) + CO(X^1\Sigma^+)$ (r_e). The diatom lies on the *x*-axis with its geometric center at the origin and the oxygen atom on the left side in the upper panel and on the right in the lower one. The position of the third atom corresponds with the cartesian (*x*, *y*) coordinates.

reaction leading to CH + O is endothermic. This figure clearly shows the presence of a deep well of more than 5.4 eV when the carbon atom approaches OH on the oxygen side. It leads to the formation of COH for $\angle COH \approx 110°$. The symmetric conterpart is observed on the opposite side of the OH-axis with a saddle point or inversion barrier at $\angle COH = 180°$ around −4.2 eV. A similar figure for the potential energy of the products is presented in Figure 5b as a function of the position of H around CO, which lies on the *x*-axis. The CO geometric center is fixed at the origin, and the C−O distance is fixed at its equilibrium distance of 2.14 bohr. Here, the zero of energy is taken to be the output channel, i.e., $H(^2S) + CO(X^1\Sigma^+)$ ($r_e = 2.14$ bohr). This figure presents several important features of the potential of the ground X^2A' state. First, there is an attractive well (dotted contours) that corresponds to the most stable minimum of HCO. Second, there is a metastable (relative to the output channel) well that corresponds to the COH minimum. Third, we can see three saddle points, one barrier for the inversion of HCO, one barrier for the inversion of COH, and one barrier for the isomerization of HCO into COH. As will be discussed later, at the top of the HCO inversion barrier, the ground electronic state becomes degenerate with an excited electronic state, the $1^2A''$ state, and these two states form the two components of a Renner−Teller pair. The third minimum

TABLE 4: Calculated Structures, Normal-Mode Frequencies (in cm^{-1}), and Relative Energies (in eV) for the Two Minima

parameter	present surface	others
	HCO Minimum	
E (eV) relative to H + CO	−0.78	−0.84,[a] −0.81,[b,g] −0.834(−0.784)[c]
E (eV) relative to C + OH	−7.26	
R_{CH} (bohr)	2.10	2.12,[a,b,g] 2.11,[c] 2.10[d]
R_{CO} (bohr)	2.24	2.26,[a] 2.24,[b,g] 2.23,[c] 2.21[d]
∠HCO (deg)	126	124,[a] 126,[b,g] 124.5,[c] 127.43[d]
ω_1 (cm^{-1}) (CH stretch)	2767	2748,[a] 2920,[b] (2456),[c] 2434.5,[e] 2435[f]
ω_2 (cm^{-1}) (CO stretch)	1885	1905,[a] 2147,[b] (1843.2),[c] 1868,[e] 1875[f]
ω_3 (cm^{-1}) (HCO bend)	1142	1145,[a] 1148,[b] (1079.2),[c] 1080.8,[e] 1101[f]
(R (bohr), r (bohr), θ(deg))	(2.03, 3.87, 151)	
	COH Minimum	
E (eV) relative to H + CO	0.99	0.84,[a] 1.04[b,g]
E (eV) relative to C + OH	−5.50	
R_{OH} (bohr)	1.85	1.85[a,b,g]
R_{CO} (bohr)	2.44	2.45,[a] 2.43[b,g]
∠COH (deg)	111	112,[a] 114[b,g]
ω_1 (cm^{-1}) (OH stretch)	3495	3628,[a] 3620[b,g]
ω_2 (cm^{-1}) (CO stretch)	1387	1387,[a] 1305[b,g]
ω_3 (cm^{-1}) (COH bend)	1157	1185,[a] 1043[b,g]
(R (bohr), r (bohr), θ (deg))	(2.48, 1.85, 67)	

[a] Ref 4. [b] Refs 6, 7. [c] Ref 1. [d] Ref 25. [e] Ref 26. [f] Ref 27. [g] Ref 18.

and the other two saddle points (one barrier for the dissociation of HCO into H + CO and one barrier for the dissociation of COH into CO + H) are more clearly seen in Figure 6a and b for $\theta = 65°$ and $\theta = 150°$, respectively, corresponding to the Jacobi angle of the respective minima (see Table 4). Similar figures for $\theta = 0°$ (Figure 6c) and $\theta = 180°$ (Figure 6d) show that the title reaction will be energetically possible through an abstraction mechanism when carbon approaches the hydroxyl radical on the oxygen side, while the dissociation channel CH + O will not be possible at low energy due to a huge potential barrier when the carbon approaches OH on the hydrogen side ($\theta = 180°$). To conclude with this triatomic system, the ground X^2A' PES presents three minima and five saddle points described well by the present RKHS global fit. Their numerical characteristics have been tabulated in Table 4 for the first two minima and in Table 5 for the five saddle points. Energetics of these extrema relative to the entrance and output channels of the title reaction are presented in the lower panel of Figure 7, while their electronic structure is visualized in the upper panel.

To demonstrate how well our fit behaves, expecially near the conical intersection, we present in Figure 8 one-dimensional cuts through the PES along ∠HCO (Figure 8a) and R_{CH} (Figure 8b) for fixed CO distance of 2.05 bohr. For this value of R_{CO}, the conical intersection occurs near $R_{CH} \approx 2.5$ bohr as clearly shown by the upper curve obtained for this CH distance in Figure 8a. With increasing distance from the conical intersection, in both directions, the potential cuts become gradually smoother. The same general behavior is also seen in Figure 8b. With increasing distance away from the linear geometry, the potential cuts become more and more smooth. Figure 8b nicely illustrates that the potential barrier to dissociation of HCO (the H−CO saddle point) at $\angle HCO \approx 120°$ is essentially a remnant of the conical intersection at 180°.

C. Comparison with Previous Potential Energy Surfaces. Four previous semiempirical and ab initio calculations of the ground HCO/COH potential energy surface exist but are limited to short distances in CO, as they were built up for the description

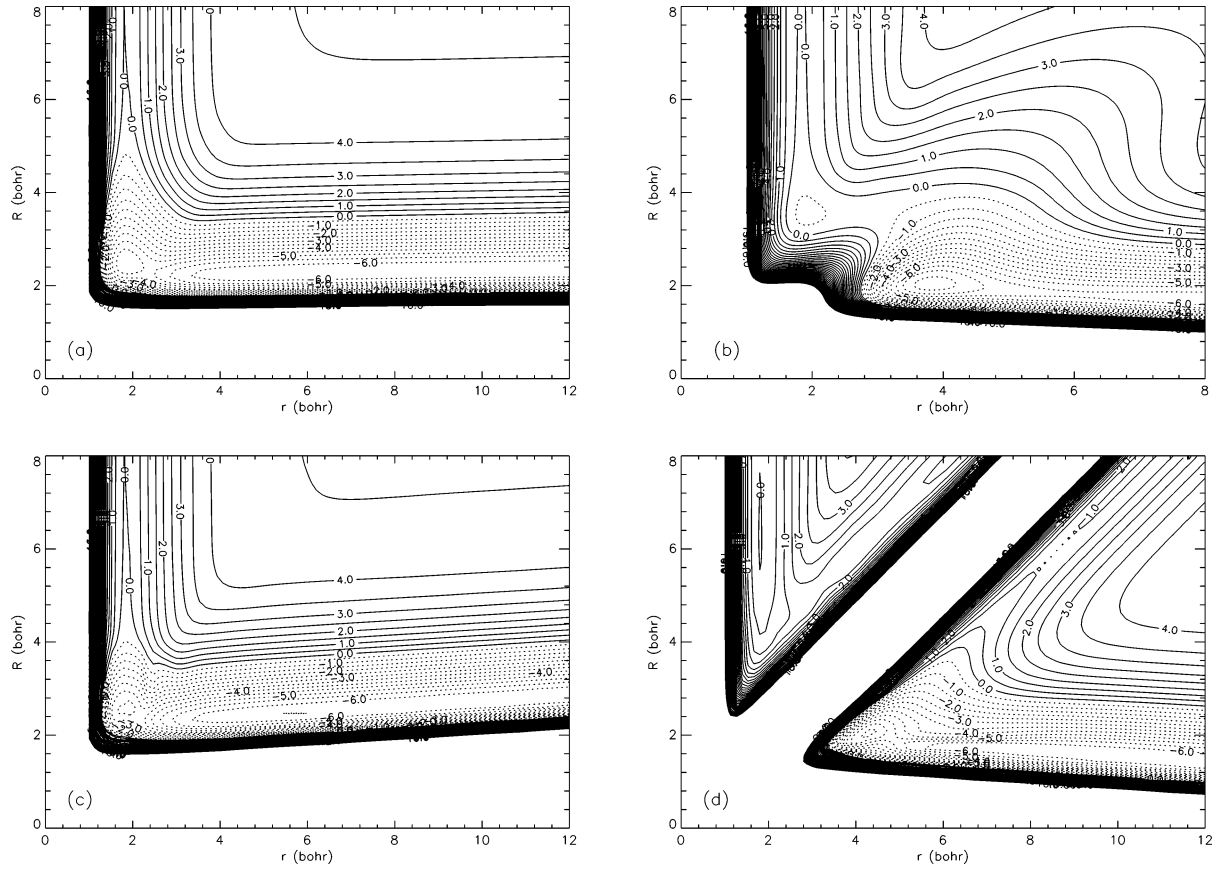

Figure 6. Contour plots of the X^2A' state of HCO/COH as a function of the Jacobi R and r_{OH} coordinates with (a) $\theta = 65°$, (b) $\theta = 150°$, (c) $\theta = 0°$, and (d) $\theta = 180°$.

of the H + CO system or photodissociation of HCO into H + CO. Indeed, the first PES was semiempirical and published by Carter et al.[5] more than 25 years ago. Another one was fitted by Geiger and Schatz[6,7] with the Sorbie−Murrell (SM) method on configuration interaction calculations of Dunning[18] for limited portions of the PES. The first (semi)global ab initio PES (with a small semiempirical adjustment) was proposed by Bowman, Bittman, and Harding (BBH)[4] 20 years ago but limited to $R_{CO} \leq 3.4$ bohr. More recently, new ab initio (semi)global PESs for the first three states, $(1,2)^2A'$ and $1^2A''$ of HCO/COH, were built up by Werner and colleagues[1,13] at a high computational level (MR-SDCI) followed by a high-precision fitting procedure in order to study the photodissociation of HCO into H + CO. Again, the range of C−O distances is limited to values lower than 3.0 bohr. Despite the high level of calculations used by these authors, deviations observed with the experimental values for the two stretching modes (CH and CO), the dissociation barrier of HCO to H + CO, and the dissociation energy of HCO force the authors to slightly adjust the PES to better fit the experimental characteristics, following the high sensitivity of the width and positions of their resonances to these features. Despite all these refinements, their PES remains inadequate for the present purpose which requires a fully global surface in order to correctly describe the entrance channel of the title reaction and so requires the characterization of the region with large C−O distances. We compare in Tables 4 and 5 present results with those of previous works in order to check the quality of our calculations.

In good agreement with the unmodified PES of Werner and colleagues[13] and similar to them, we get a dissociation energy for HCO that is too small, while its equilibrium structure (R_{CO}, R_{CH}, ∠HCO) is in good agreement with the experimental values of Austin et al.[25] The first excitation energies of the two stretching CH and CO and bending modes are all overestimated relative to the experimental values[26] (+14%, less than 1% and 6%, respectively), while they are in good agreement with the adjusted PES of Bowman et al.[4] So, the present PES will lead to a zero-point dissociation energy, D_0^0 (measured from the zero-point level of HCO to the zero-point level of H + CO), that is too small, due to the cumulative contributions of the potential well that is too shallow with vibrational frequencies that are too high. The most recent experimental value of the zero-point dissociation energy is 0.603 eV, derived in ref 13 from the room-temperature bond enthalpy for HCO → H + CO measured by Chuang et al.[30] Thus, our calculated dissociation energy is too small by about 0.06 eV. Another crucial characteristic for the photodissociation or collision excitation of H with CO is the barrier to dissociation/formation of HCO to/from H + CO. The experimental value of this HCO → H + CO barrier is very small relative to H + CO (0.087 eV according to Wang et al.[29]) and is, in all cases, widely overestimated (by +0.06 eV in present work) unless improved by empirical adjustements, while the position of this barrier is in good agreement with the recent determination of Werner and colleagues.[1] The barrier of HCO at linearity (at 180°) has an energy of +0.31 eV relative to H + CO, i.e., the barrier height is 1.09 eV with respect to the depth of the well. This linear saddle point corresponds to the minimum of the $\tilde{A}^2A''$ (equivalent at 180° to the $^2\Pi$ state), and its geometry is known from the spectroscopic work of Johns et al.:[28] $R_{CH} = 2.012$ bohr, and $R_{CO} = 2.258$ bohr.

The COH part of the PES is less known, as this complex has never been observed experimentally. Only theoretical investiga-

TABLE 5: Calculated Structures, Normal-Mode Frequencies (in cm^{-1}), and Relative Energies (in eV) for the Five Saddle Points

parameter	present surface	others
H−CO Saddle Point		
E (eV) relative to H + CO	0.15	0.069,[a] 0.11,[b,f] 0.125(0.169),[c] 0.087[e]
E (eV) relative to C + OH	-6.34	
R_{CH} (bohr)	3.46	3.43,[a] 3.35,[b] 3.53,[c] 3.26[f]
R_{CO} (bohr)	2.15	2.19,[a] 2.18,[b] 2.15,[c] 2.17[f]
∠HCO (deg)	115	117,[a] 139,[b] 117.0,[c] 118[f]
(R (bohr), r (bohr), θ (deg))	(1.95, 4.79, 134)	
HCO Inversion Saddle Point		
E (eV) relative to H + CO	0.31	0.39,[a] 0.27(0.31)[c]
E (eV) relative to C + OH	-6.18	
R_{CH} (bohr)	2.01	2.03,[a] 2.01,[c] 2.012[d]
R_{CO} (bohr)	2.30	2.28,[a] 2.25,[c] 2.258[d]
∠HCO (deg)	180	180[a,c,d]
(R (bohr), r (bohr), θ (deg))	(2.04, 4.31, 180)	
CO−H Saddle Point		
E (eV) relative to H + CO	1.46	1.46,[a] 1.72[b,f]
E (eV) relative to C + OH	-5.03	
R_{OH} (bohr)	2.32	2.31,[a] 2.53,[b] 2.33[f]
R_{CO} (bohr)	2.26	2.26,[a] 2.33,[b] 2.26[f]
∠COH (deg)	120	119,[a] 125,[b] 120[f]
(R (bohr), r (bohr), θ (deg))	(2.33, 2.32, 57)	
COH Inversion Saddle Point		
E (eV) relative to H + CO	2.26	2.36[g]
E (eV) relative to C + OH	-4.23	
R_{OH} (bohr)	1.95	
R_{CO} (bohr)	2.46	
∠COH (deg)	180	
(R (bohr), r (bohr), θ (deg))	(2.58, 1.95, 0)	
Isomerization Saddle Point		
E (eV) relative to H + CO	2.04	2.11,[a] 2.64,[b] 2.30[f]
E (eV) relative to C + OH	-4.44	
R_{CH} (bohr)	2.48	2.49,[a] 2.83,[b] 2.51[f]
R_{CO} (bohr)	2.40	2.45,[a] 2.30,[b] 2.43[f]
∠HCO (deg)	52.8	51.7[a]
(R (bohr), r (bohr), θ (deg))	(2.35, 2.17, 112)	

[a] Ref 4. [b] Ref 6, 7. [c] Ref 1. [d] Ref 28. [e] Ref 29. [f] Ref 18. [g] Ref 5.

tions have been performed on it.[4,5,7] In particular, COH is predicted to be metastable with a minimum at 1.00 eV above the CO + H asymptote with a barrier to dissociation of 0.46 eV (or a barrier of formation of 1.46 eV relative to H + CO). The structural characteristics of all these extrema are seen to be in good agreement with previous findings, though the COH inversion saddle point was not characterized before except by a semiempirical study of Carter et al.[5] more than 25 years ago. Indeed, Bowman et al.[4] found that it was too high in energy above the CO + H asymptote to be considered, while it will contribute to the title reaction, as it appears lower than the entrance channel, i.e., −4.23 eV relative to C + OH.

V. Reaction Path

While it is not possible to plot the PES in three dimensions and as partial 2D cuts of the PES with a fixed third coordinate usually give an energetically nonoptimized view of the PES, we have plotted minimum-energy reaction paths of the title reaction in three cases: first, when the path goes through the absolute HCO minimum of the PES; second, when the path goes through the metastable COH minimum; third, in the case of an abstraction linear reaction again via COH. The reaction path (RP) going through the global minimum has been obtained by following the steepest descent from both entrance and exit channels to the global minimum. It is thus equivalent to the minimum energy path (MEP). The other two have been evaluated using Quapp's growing string (GS) method.[31] They

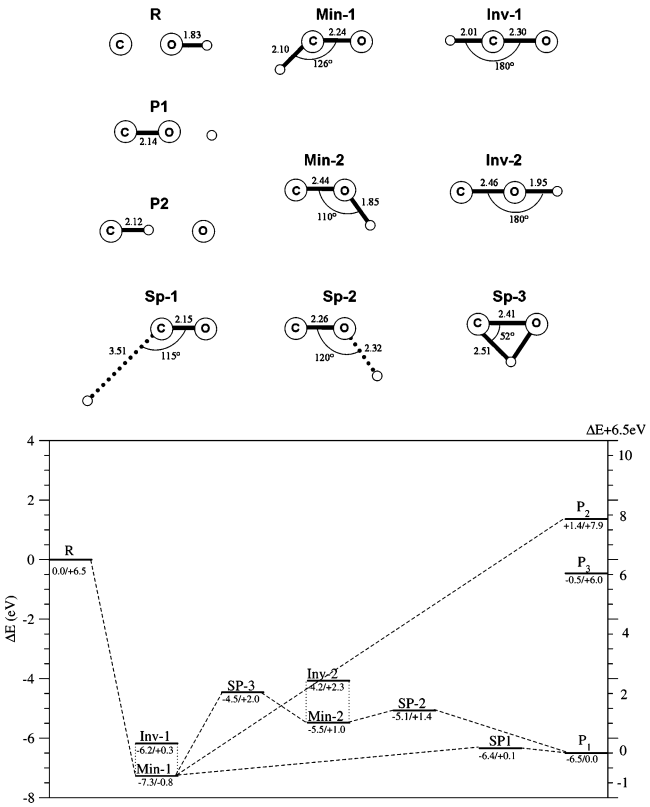

Figure 7. Lower panel: Energetic diagram of the stationary points located on the analytical PES of the HCO/COH X^2A' state. Energies (in eV) are given relative to the reactants (left) or to the products (right). Upper panel: Optimized geometries (in bohr, deg) of the corresponding stationary points of the complex. The smallest circle represents the H atom. The P3 structure, which is an excited state of P1, is not described here as it is not related to this PES.

are not equivalent to MEPs, since they are not the steepest descent from a saddle point. However, an appropriate RP is not necessarily equivalent to the MEP,[32] and the trajectories followed by the GS method connect two minima by passing through one saddle point.[1] Thus, these two RP are good approximations of the local MEPs in the corresponding region of the PES.

These three MEPs are plotted in Figure 9a. The barriers to dissociation of HCO and COH into H + CO are clearly seen as well as a metastable minimum for the linear abstraction corresponding to the inversion saddle point of COH (see also Figure 9b). For these three cases, the reaction will be possible with no potential barrier energetically higher than the entrance channel.

VI. Conclusion

The entrance channel of the $C(^3P) + OH(X^2\Pi)$ reaction gives rise to six doublet states($(1-3)^2A'$, $(1-3)^2A''$) and six quartet states ($(1-3)^4A'$, $(1-3)^4A''$). Due to the nondegenerate case of the output $CO(X\ ^1\Sigma_g^+) + H(^2S)$ channel, only one among those twelve states correlates with the product channel, i.e., the X^2A'. Furthermore, most of them have a repulsive behavior in the entrance channel. Nevertheless, a crossing between Π and Σ states in $C_{\infty v}$ gives rise to avoided crossing for nonlinear geometries and extrema on the surfaces. For obvious reasons, we have considered in a first step only the state that correlates to both the reactant and product channels.

We have built up a new fully global potential energy surface for this X^2A' state allowing the treatment of the reactive $C(^3P) + OH(X^2\Pi) \rightarrow CO(X^1\Sigma_g^+) + H(^2S)$ collision based on the ab

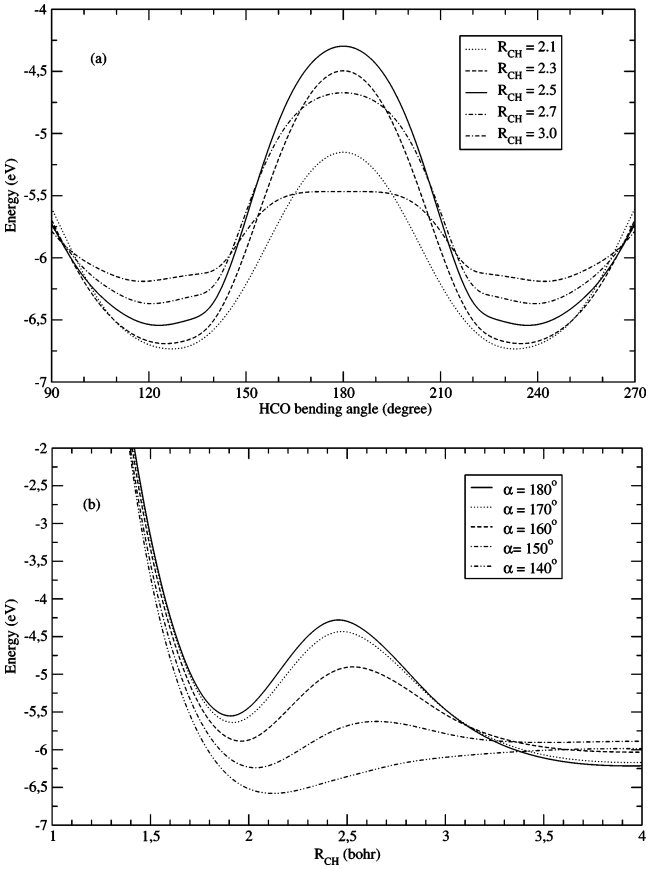

Figure 8. (a) Potential cuts along the H−C−O bending angle for several values of the CH bond distance (in bohr) as indicated. The C−O distance is fixed at $R_{CO} = 2.05$ bohr. (b) The same as in (a) but for cuts along the CH separation R_{CH} for fixed values of $\alpha = \angle$HCO.

initio multireference (MR) internally contracted single and double configuration interaction (SDCI) method plus Davidson correction (+Q) using Dunning aug-cc-pVQZ basis sets. In particular, the multireference space is taken to be a complete active space (CAS). Improvement over previously proposed potential energy surfaces for HCO/COH is obtained in the sense that the present surface also describes the potential part where the interatomic distance of CO is large. The $C(^3P) + OH(X^2\Pi) \rightarrow CO(X^1\Sigma^+) + H(^2S)$ reaction is highly exothermic with a ΔH_0^0 around 6.4 eV.

A large number of geometries (∼2000) have been calculated and analytically fitted using the reproducing kernel Hilbert space (RKHS) method of Ho and Rabitz both for the two-body and three-body terms following the many-body decomposition of the total electronic energies. Three minima and five saddle points are observed on this surface, described in the present study, and found to be in good agreement with previous work. The minima correspond to the formation of the HCO and COH complexes and to the CO + H products, with the COH complex being a metastable minimum relative to the product channel. The saddle points correspond to potential barriers for both the dissociation/formation of HCO and COH into/from CO + H, to a barrier for the isomerization of HCO into COH, and to barriers for the inversion of HCO and COH through their respective linear configuration. Following the strong exothermicity of the reaction, these barriers should play a minimal role during the reaction, while the global reaction is found barrierless (relative to the reactant channel). A dynamical study of the title reaction using quasi-classical trajectory calculations on this PES is being performed in our group and will be presented in a following paper.

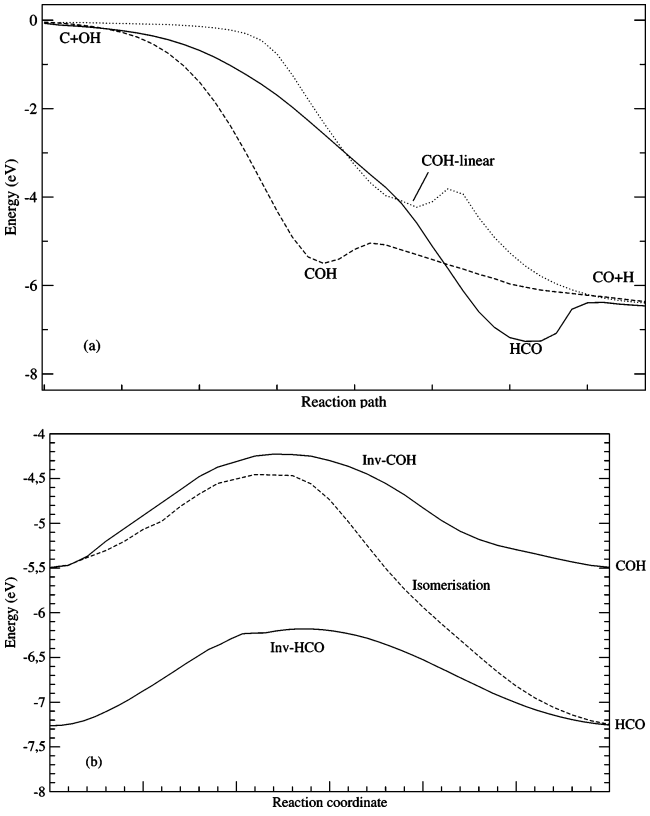

Figure 9. Minimum-energy paths for (a) the $C(^3P) + OH(X^2\Pi) \rightarrow CO(X^1\Sigma^+) + H(^2S)$ reaction; (b) the inversion and isomerization pathways of HCO/COH in the ground X^2A' state.

Acknowledgment. We would like to thank the Institut du Développement et des Ressources en Informatique Scientifique (IDRIS, CNRS) for providing us with the computer power as well as the "Pole de Calcul informatique de l'Ouest (PCIO)". Furthermore, the authors and, in particular, A.Z. thank Andrea Simoni and Philippe Halvick for their judicious advice during the realization of this work.

References and Notes

(1) Keller, H.-M.; Floethmann, H.; Dobbyn, A. J.; Schinke, R.; Werner, H.-J.; Bauer, C.; Rosmus, P. *J. Chem. Phys.* **1996**, *105*, 4983.
(2) Loettgers, A.; Untch, A.; Keller, H.-M.; Schinke, R.; Werner, H.-J.; Bauer, C.; Rosmus, P. *J. Chem. Phys.* **1997**, *106*, 3186.
(3) Loettgers, A.; Untch, A.; Stumpf, M.; Schinke, R.; Werner, H.-J.; Bauer, C.; Rosmus, P. *Chem. Phys. Lett.* **1994**, *230*, 290.
(4) Bowman, J. M.; Bittman, J. S.; Harding, L. B. *J. Chem. Phys.* **1986**, *85*, 911.
(5) Carter, S.; Mills, I. M.; Murrell, J. N. *J. Chem. Soc., Faraday Trans. 2* **1979**, *1*, 148.
(6) Geiger, L. C.; Schatz, G. C. *J. Phys. Chem.* **1984**, *88*, 214.
(7) Geiger, L. C.; Schatz, G. C.; Harding, L. B. *Chem. Phys. Lett.* **1985**, *114*, 520.
(8) Romanowski, H.; Lee, K.-T.; Bowman, J. M.; Harding, L. B. *J. Chem. Phys.* **1986**, *84*, 4888.
(9) Bussery-Honvault, B.; Honvault, P.; Launay, J.-M. *J. Chem. Phys.* **2001**, *115*, 10701. Bussery-Honvault, B.; Julien, J.; Honvault, P.; Launay, J.-M. *Phys. Chem. Chem. Phys.* **2005**, *7*, 1.
(10) Honvault, P.; Launay, J.-M. *J. Chem. Phys.* **2001**, *114*, 1057.
(11) Honvault, P.; Launay, J.-M. *J. Chem. Phys.* **1999**, *111*, 6665.
(12) Honvault, P.; Launay, J.-M. *Chem. Phys. Lett.* **2003**, *370*, 371.
(13) Werner, H.-J.; Bauer, C.; Rosmus, P.; Keller, H.-M.; Stumpf, M.; Schinke, R. *J. Chem. Phys.* **1995**, *102*, 3593.
(14) Ho, T.-S.; Hollebeck, T.; Rabitz, H.; Harding, L. B.; Schatz, G. C. *J. Chem. Phys.* **1996**, *105*, 10472.
(15) Dayou, F.; Spielfiedel, A. *J. Chem. Phys.* **2003**, *119*, 4237.
(16) Boggio-Pasqua, M.; Halvick, Ph.; Rayez, M.-T.; Rayez, J.-C.; Robbe, J.-M. *J. Phys. Chem.* **1998**, *102*, 2009. Boggio-Pasqua, M.; Voronin, A. I.; Halvick, Ph.; Rayez, J.-C. *Phys. Chem. Chem. Phys.* **2000**, *2*, 1693.
(17) Amos, R. D.; Bernhardsson, A.; Berning, A.; Celani, P.; Cooper, D. L.; Deegan, M. J. O.; Dobbyn, A. J.; Eckert, F.; Hampel, C.; Hetzer,

G.; Knowles, P. J.; Korona, T.; Lindh, R.; Lloyd, A. W.; McNicholas, S. J.; Manby, F. R.; Meyer, W.; Mura, M. E.; Nicklass, A.; Palmieri, P.; Pitzer, R.; Rauhut, G.; Schütz, M.; Schumann, U.; Stoll, H.; Stone, A. J.; Tarroni, R.; Thorsteinsson, T.; Werner, H.-J. *MOLPRO*, a package of ab initio programs designed by H.-J. Werner and P. J. Knowles, version 2002.6; http://www.molpro.net.

(18) Dunning, T. H. J. *J. Chem. Phys.* **1980**, *73*, 2304.

(19) Huber, K. P.; Herzberg, G. In *Molecular Spectra and Molecular Structure IV. Constants of Diatomic Molecules*; van Nostrand: New York, 1979.

(20) Herzberg, G. In *Spectra of Diatomic Molecules, Molecular Spectra and Molecular Structure*; van Nostrand: New York, 1959.

(21) Scientific and technical databases of the National Institute of Standards and Technology; http://physics.nist.gov/PhysRefData/ (accessed Sept 2006).

(22) Murrell, N.; Carter, S. *J. Phys. Chem.* **1984**, *88*, 4887.

(23) Ho, T.-S.; Rabitz, H. *J. Chem. Phys.* **1996**, *104*, 2584.

(24) Hollebeek, T.; Ho, T.-S.; Rabitz, H. *J. Chem. Phys.* **1997**, *106*, 7223.

(25) Austin, J. A. Levy, D. H.; Gottlieb, C. A.; Radford, H. E. *J. Chem. Phys.* **1974**, *60*, 207.

(26) Milligan, D. E.; Jacox, M. E. *J. Chem. Phys.* **1969**, *51*, 277.

(27) Sappey, A. D.; Crosley, D. R. *J. Chem. Phys.* **1990**, *93*, 7601.

(28) Johns, J. W. C.; Priddle, S. H.; Ramsay, D. A. *Discuss. Faraday Soc.* **1963**, *35*, 90.

(29) Wang, H. Y.; Eyre, J. A.; Dorfman, L. M. *J. Chem. Phys.* **1973**, *59*, 5199.

(30) Chuang, M.-C.; Foltz, M. F.; Moore, C. B. *J. Chem. Phys.* **1987**, *87*, 3855.

(31) Quapp, W. *J. Chem. Phys.* **2005**, *122*, 174106.

(32) Ammel, S. C.; Yamataka, H.; Aida, M.; Dupuis, M. *Science* **2003**, *200*, 1555.